Application of silica-based sorbents to extraction of rare earth elements from loparite processing products

A. V. Muslimova, *Associated Professor, Department of Chemistry and Technology of Modern Energy Materials*[1], *e-mail: klameri7@gmail.com*
A. S. Bujnovskij, *Professor, Department of Chemistry and Technology of Modern Energy Materials*[1]
N. I. Karakchieva, *Senior Researcher*[2, 3], *e-mail: karakchieva@mail.tsu.ru*
V. I. Sachkov, *Professor, Head of the Laboratory "Innovation and Technology Center"*[2], *e-mail: itc@spti.tsu.ru*

[1] *Seversk Technological Institute, a branch of State Autonomous Educational Institution of Higher Education National Research Nuclear University MEPhI, Seversk, Russia.*
[2] *National Research Tomsk State University, Tomsk, Russia.*
[3] *Siberian Research Institute of Agriculture and Peat-branch of Siberian Federal Scientific Centre of Agro-biotechnologies of The Russian Academy of Sciences, Tomsk, Russia.*

Apatite and loparite are the main sources of rare earth elements (REE) in Russia. Loparite is a complex titanate and niobate containing up to 30% wt. of REE oxides predominantly of the cerium group. Extraction processing methods are used at the stages of group separation and separation of REE concentrates. Tributyl phosphate (TBP) is a widely used extracting agent for these purposes. Extraction technologies have a number of disadvantages, in particular, a large number of separation stages because of low separation coefficients of individual REE combined with difficulties in separating liquid phases. The use of TBP-containing sorbents allows to eliminate the latter disadvantage. Both organic polymers and inorganic compounds may be used as sorbent carriers; among inorganic ones, silica is widely used, and it was selected for this study. The purpose of this work was to study the effect of variations of the proposed methods for synthesis of silica and modified TBP based sorbents on their ability to extract REE from the solutions of loparite concentrate processing. The article briefly describes a procedure for sorbent samples synthesis. Tetraethoxysilane, tributyl phosphate, stannic chloride and nanotubes have been used as starting reagents for the synthesis. A number of physicochemical properties have been determined for the synthesized samples (pore volume and their average diameter, surface area and morphology, acid-base properties of the surface), and thermogravimetric analysis has been performed. The sorption properties of the samples have been tested by the example of REE extraction from process solutions of loparite working up. The separation coefficients of Sm/La pairs up to 3.7, Pr/Nd up to 1.8 were obtained; therefore, the studied samples may be potentially used for samarium isolation from the REE combination, as well as for Pr – Nd pair separation.

Key words: loparite, rare earth elements, thorium, separation, sorbents, tributyl phosphate, silica, stannic chloride.
DOI: 10.17580/nfm.2022.01.03

Introduction

Rare earth elements (REE) are a group of elements of the periodic table that have unique physical properties, which makes the applications of REE-based compounds very extensive. The proximity of chemical properties and presence of accompanying actinides in natural raw materials keep the issues of their purification and separation topical for many years. The most well–known and widely used method of REE isolation and separation is an extraction using tributyl phosphate, di(2-ethylhexyl) phosphoric acid, salts of quaternary ammonium bases or mixtures of extracting agents.

In Russia, the main sources of REE are apatite and loparite. Loparite is a complex oxide of titanium and niobium containing up to 30% wt. of REE oxides, mainly of the cerium group [1]. Processing of the Lovozero deposit loparite ores (Murmansk, Russia) is carried out at the Solikamsk Magnesium Plant [2]. According to the industrially mastered chlorine technology, niobium, titanium and tantalum compounds are first isolated, and then a collective carbonate concentrate of REE is isolated as well [3]. The advantage of loparite is the relatively low content of actinides in it: the total activity of the commercial REE concentrate does not exceed 1000 Bq/kg [4]. Afterpurification, group separation, isolation of individual oxides by extraction methods have been developed at different times at the Irtysh Chemical-Metallurgical Plant (Kazakhstan) [1, 5], the Sillamäe Plant (Estonia) [5–6], Chemical and Metallurgical Experimental Workshop (Verkhnyaya Pyshma, Russia) [2], at the moment — Skygrad Group of Companies (Russia) [2, 7].

Extraction technologies have a number of significant limitations, in particular, a large number of separation steps along with the difficulty in separating liquid phases [8], which is of particular importance for REE separation processes, where the use of undiluted TBP with high viscosity and density close to the density of the aqueous phase is often required. This imposes some restrictions on

the extraction conditions and complicates the hardware design of the process.

It is possible to get over the limitations by using TBP-based sorbents [9–10], and solid extractants (TVEX) in which TBP is non-covalently bound to a solid carrier [8, 11–12]. Both organic polymers and inorganic compounds (for example, widely applied silica) can be used as a matrix or carrier [13–14].

It is known that the extraction properties of neutral oxygen–containing compounds grow significantly with an increase in oxygen basicity (for TBP — a phosphoryl oxygen atom), leading to a rise in the oxygen reactivity [15]. This can be achieved by replacing the substituents or the reaction center itself in TBP (for example, with AsO or SbO [15]). Therefore, it is proposed to use tetraethoxysilane and stannic chloride for realkylation of TBP during the synthesis. Stannic chloride can also be a polymerization catalyst, and under certain conditions, it can be implanted into the polysiloxane skeleton [16].

Another disadvantage of TBP, which limits its application in REE separation into individual components, is low separation coefficients of the neighboring element pairs. This force to use the displasing extraction schemes [17–18], when part of the output concentrates returns to the stage of washing or saturation of the extractant: the lower is the separation coefficient, the relatively larger amount of concentrate have to be returned to the process, and, accordingly, less amount is removed from the scheme as concentrate. Tin chloride forms extraction compounds with TBP ($SnCl_4 \cdot n$TBP and $H_2SnCl_6 \cdot n$TBP, where $n = 2$ or 3 [19]), so when it is added to the system, one can expect that extraction may follow a displacement mechanism without applying pure REE concentrates: more extractable compounds will displace tin into solution, and less extractable ones will remain in the raffinate.

Tin chloride in aqueous solutions is exposed to hydrolysis with formation of a thin film of stannic oxide on the surface of the particles, and the resulting film can serve as a TBP fixing agent on the sorbent matrix surface and a diffusion barrier [20]; the latter may contribute to an increase in REE separation coefficients. Silica modified with tin chloride can acquire the properties of cation exchangers [20].

It was proposed to introduce nanotubes into the composition of synthesized samples as a reinforcement additive in order to improve their physico-mechanical properties [21].

Thus, the purpose of this work was to study the effect of variations of the proposed methods for synthesis of silica and modified TBP based sorbents on their ability to extract REE from the solutions of loparite concentrate processing.

The use of the obtained sorbents in the hydrometallurgical industry can reduce the number of stages of sequential purification and of column devices, increase the productivity of individual devices, reduce the specific consumption of elution solutions, salting-out agents and production waste, which finally will lead to a reduction of production costs.

Materials and methods

Materials. Tetraethylorthosilicate – TEOS (reagent grade), tributyl phosphate – TBP (pure for extraction), stannic chloride – TTC (analytical), multi-wall carbon nanotubes (Baytubes C 150 P, Bayer), and distilled water were used for the synthesis of samples.

The working solution for investigating REE extraction was prepared by dissolving the total concentrate of REE carbonates isolated from loparite (the content of REE oxides is 44.8% wt; Solikamsk Magnesium Plant), dried to a constant mass at 110 °C, in concentrated nitric acid (OSCh 27-4, GOST 11125). The pH value of the solution was brought to 1.0 with nitric acid solutions (1 M and 0.1 M) to simulate highly acidic process solutions.

Indicator solutions with a concentration of 1.5×10^{-4} mol/dm^3 were used for indicator analysis (in parentheses there are indicated in order: the acidity index value; the wavelength of maximum absorption, nm; the indicator solution volume added during the analysis, cm^3): o-nitroaniline (–0.29; 400; 2.0), crystal violet (0.8; 590; 0.2), brilliant green (1.3; 590; 0.5), m-nitroanaline (2.5; 364; 1.0), methyl-orange (3.5; 440; 1.0), bromphenol blue (4.1; 590; 0.5), methyl red (5.0; 315; 1.0), chrysoidin (5.5; 440; 1.0), bromocresol purple (6.4; 590; 1.0), p-nitrophenol (7.1; 440; 1.0), bromothymol blue (7.3; 440; 1.0), thymol blue (8.8; 315; 0.5), pyrocatechol (9.45; 590; 2.0), Nile blue (10.5; 590; 0.5), indigocarmine (12.8; 400; 1.0).

Methods. When mixing starting reagents in liquid form and heating the mixtures, an IKA C-MAG HS 7 magnetic stirrer was used. To introduce nanotubes into agueous media, a UZTA-0.4/22-OM apparatus was used under the following conditions: 30 minutes, output power 90%, and frequency of ultrasonic vibrations 22±1.65 kHz. Drying of the obtained samples was carried out in a TL-VO/20 vacuum drying oven.

Analysis of REE-containing solutions was carried out using an iCAP-6200 Duo atomic emission spectrometer; the pH level was monitored using a pH-410 device.

The following physicochemical properties of the synthesized samples were determined: specific surface area – using BET multipoint measurement method by low–temperature nitrogen adsorption, volume and pore size on the surface – by the Barrett–Joyner–Halenda model at relative pressure of $p/p_0 = 0.99$ using a TriStar 3020 analyzer; topographic analysis of the surface – using a secondary electron detector; microanalysis was implemented using a Sapphire *X*-ray detector of a Quanta 200 3D microscope. The acid-base properties of the sample surface were studied by indicator analysis with the use of a KFK-2 photocolorimeter in 1 cm long cuvettes in the spectral range of 315–590 nm in the range of acid-base strength *pKa* from (–0.29) to 12.8.

The indicator analysis was carried out in the following order: weighted specimens of 0.02 g were placed into measuring tubes with a capacity of 5 cm^3, a certain volume of the indicator solution was poured, then it was brought to the mark with distilled water and kept for 2 hours until the adsorption equilibrium was established; at the same time, a blank experiment was carried out. The concentration of active centers of this force, equivalent to the adsorbed dye amount, was calculated by the following formula:

$$q(pKa) = C_i \cdot V_i \cdot [|(D_0 - D_1)/a_1 \pm (D_0 - D_2)/a_2|]/D_0, \quad (1)$$

where $q(pKa)$ is the concentration of active centers of a given force, mol/ g; C_i and V_i are the concentration and volume of the indicator with a certain acidity pKa, mol/dm^3 and cm^3, respectively; D_0, D_1, D_2 are the optical density of the indicator solution before sorption, after sorption, in the blank experiment; a_1 and a_2 are the weighted specimens in the working and blank experiments, g.

In formula (1), the sign "–" corresponds to a unidirectional change of D_1 and D_2 relative to D_0, and "+" corresponds to multidirectional one.

To construct kinetic hydration curves of the samples in "pH – time t" coordinates, 100 cm^3 of bidistilled water was first injected into the potentiometric cell, and after stabilization of the pH meter readings (pH-150MI with a glass electrode EMF), a weighted specimen (1 g) was added with continuous suspension stirring on a magnetic stirrer.

The kinetic curve for sample *II* failed to be obtained.

Thermogravimetric analysis was performed on a STA 409 PC Luxx synchronous thermal analyzer at heating rate of 5 °/min to 1000 °C, weight of the sample (15 ± 1) mg (26 mg for sample *II*), medium – air (40 cm^3/min), crucible material – Al_2O_3.

Synthesis of sorbent samples. Volume ratios of the starting reagents for samples *I* and *III* – TEOS : TBP: TTC: H_2O = 14 : 20 : 2 : 10, for sample *II* – 13.3 : 20 : 7.8 : 5. The sequence of TBP and TTC addition has been varied. The order of synthesis is as follows:

1) introduction of carbon nanotubes into one of the reagents using ultrasonic exposure for their uniform distribution. Sample *I* was synthesized without addition of carbon nanotubes; for synthesizing of sample *II* and sample *III*, 10 mg of nanotubes were introduced into TBP and 7 mg of nanotubes into TEOS, respectively;

2) mixing of reagents in a certain order; the mixture was stirred for 10 minutes after adding each reagent. Mixing order for sample *I*: TEOS was added to TTC, TBP was introduced into the resulting mixture. Mixing procedure for sample *II*: TTC was added to TBP with nanotubes, then a separately prepared aqueous solution of TEOS (72.7 vol. %); went to point 5 of the synthesis order, skipping points 3-4. Mixing order for sample *III*: TBP and TTC were in tandem introduced into TEOS with nanotubes;

3) heating the mixture to 70 °C for 3 hours with constant stirring;

4) addition of water (10 cm^3);

5) polycondesation with the formation of an inorganic polymer mesh of type type ≡ Si – O – Si ≡ during the sol maturation till the material hardening (up to 168 hours);

6) filtration of synthesis products on a water-jet pump and vacuum drying of the material for 48 hours at 90 °C.

The yield was 7.95 g for sample *I*, 19.15 g for sample *II*, and 7.45 g for sample *III*. Because of high viscosity of sample *II*, the specific surface area, volume and pore size on the surface have not been determined for it, and the kinetic hydration curve was not obtained as well.

Studies on REE extraction by sorbent samples were carried out under static conditions for 140 hours at 25 °C with periodic stirring. Weighted specimens of 1.00 ± 0.05 g were taken; they were placed into conical retorts and 100 cm^3 of the process solution were added. With the process completed, filtration was implemented, and the composition of the filtrates was analyzed. The analysis results were processed according to the following formulas:

$$a = 100 \cdot (C_0 - C) / C_0, \quad (2)$$

$$\text{CEC} = V \cdot (C_0 - C) / (1000 \cdot m), \quad (3)$$

$$k = V \cdot (C_0 - C) / (C \cdot m), \quad (4)$$

$$b_{A/B} = k_A / k_B, \quad (5)$$

where a is the element extraction degree (%); C_0 and C are the element concentration in the starting solution and equilibrium concentration (mg/dm^3); CEC is cation exchange capacity (mg/g); V is the solution volume (cm^3); m is the mass of the starting weighted specimen (g); k is the element distribution coefficient (cm^3/g); $b_{A/B}$ is the pair separation coefficient for *A/B* elements.

The starting solution composition, mg/dm^3: REE – 494; La – 138; Ce – 233; Pr – 24.5; Nd – 85.5; Sm – 6.7; Eu – 0.7; Dy – 1.1; Y – 0.6; Fe – 4.2; Al – 11.6; Th – 4.1.

Results and discussion

The results of measuring the specific surface area (S_{BET}) and porous structure of synthesized samples are shown in **Table 1**; **Fig. 1** represents the pore size distribution.

Sample *I* has a larger specific surface area and a smaller average pore size, sample *III* has a larger total pore

Table 1
Parameters of the specific surface and the porous structure of the samples

Sample number	Parameter			
	S^1_{BET}, m^2/g	Average pore size, nm	Total pore volume, cm^3/g	BET rectification interval (p/p_0)
I	432	2.83	0.306	0.05–0.30
III	384	3.50	0.337	

[1]Relative error ±10 %.

volume. Both samples can be attributed to mesoporous: the average pore size was 2.83 nm for sample *I* and 3.50 nm for sample *III*.

Images of the surface of synthesized samples are shown in **Fig. 2**.

The surface of sample *I* **(Fig. 2, *a*)** is represented by not fully formed agglomerates of rounded particles up to 10 μm in size; the pores are not visually determined. The surface of sample *II* is shaped to a lesser extent **(Fig. 2, *b*)** — it is visually represented by a continuous layer without visible pores; the shape, size of individual particles, the presence of carbon nanotubes are not determined. The surface of sample *III* **(Fig. 2, *c*)** is represented by agglomerates of unevenly distributed carbon nanotubes and rounded particles up to 5 μm in size, which form sufficiently large macropores (up to 3–5 μm).

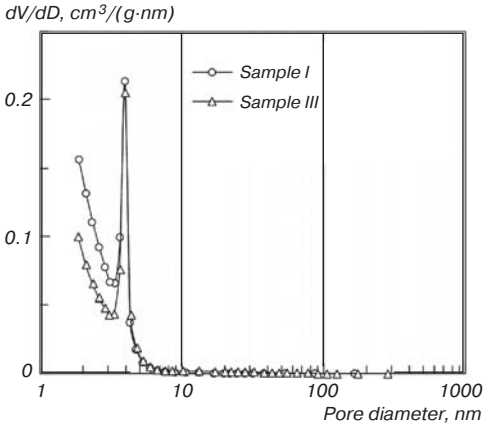

Fig. 1. Pore size distribution for samples *I* and *III*

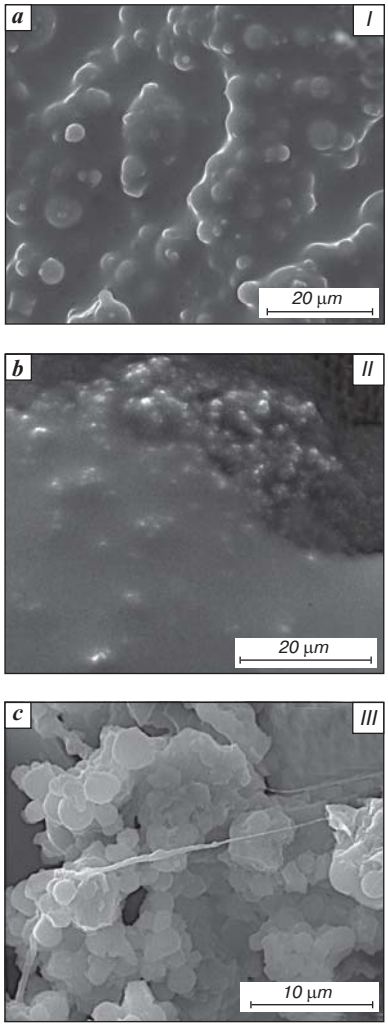

Fig. 2. Surface topography of samples

When comparing the energy dispersion spectra of the samples **(Fig. 3)**, it can be seen that the spectrum taken from the surface of sample *II* differs significantly from the others: the content of chlorine, tin, carbon and phosphorus is higher, and that of silicon is lower. The increased content of the first two elements is explained by the use of larger amount of TTC during the synthesis of this sample with the resulting covering of the matrix particles with a layer of extractant.

For samples *I* and *III*, the contents of the main elements on the surface have similar values, though the phosphorus content on the surface is slightly less for sample *II*. The results of a semi-quantitative analysis of the sample surface composition with 100% normalization are summarized in **Table 2**.

Based on the obtained results, it is possible to write the molecular formula of the sample surface compositions:

– sample *I*: $C_{90}P_{14}Si_{30}Sn_7O_{45}$;
– sample *II*: $C_{132}P_4Si_4Sn_6O_{40}$;
– sample *III*: $C_{85}P_{11}Si_{33}Sn_9O_{44}$.

Fig. 4 shows the kinetic hydration curves of samples *I* and *III*. **Fig. 4, *b*** represents the distribution spectra of adsorption centers on the sample surfaces based on the results of indicator analysis.

Table 2

The results of energy dispersion analysis of the sample surface composition

Sample number	Content, % wt.					
	C	O	Si	P	Cl	Sn
I	24.4	16.2	19.1	10.1	10.4	19.8
II	41.6	14.2	5.0	6.5	11.4	21.3
III	21.8	15.1	20.3	7.4	12.6	22.8

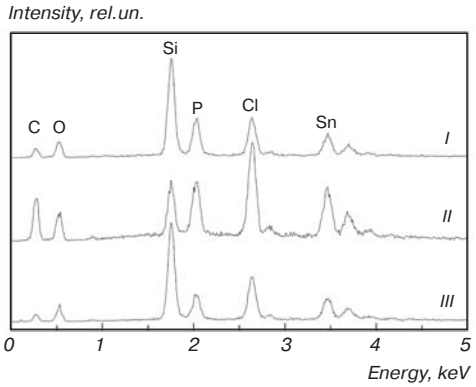

Fig. 3. Energy dispersion spectra from the surface of samples *I*-*III*

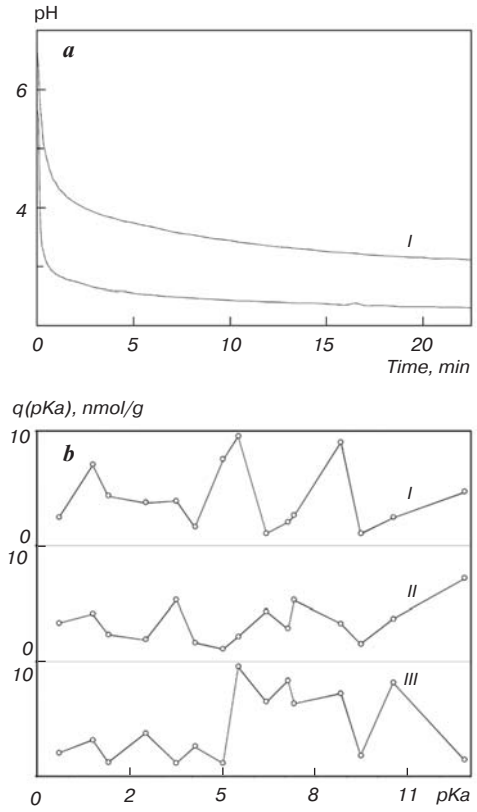

Fig. 4. The kinetic curves of pH changes in aqueous suspension of samples (*a*) and distribution spectra of adsorption centers on their surface (*b*)

The kinetic curve of pH change in the aqueous suspension of sample *I* gradually decreases to pH = 3.11 **(Fig. 4, *a*)**, which evidences the predominance of Lewis and Bröensted acid sites on the surface. The kinetic curve of the pH change of the aqueous suspension of sample *III* decreases to a pH value of up to 2.3 with a monotonous change in the first seconds of measurements.

When comparing the adsorption spectra (Fig. 4*b*), it is seen that in the *pKa* range from 0 to 5, corresponding to the Bröensted basic (E---$OH^{\delta 0}$ type, where E is an element) and acid (E---O---$H^{\delta +}$ type) sites, a low-intensity band is present on the spectrum of sample *I*. For sample *I*, two more intense bands in the *pKa* spectrum range of 4.0–6.5 and 6.5–9.5 correspond to the Bröensted acid (E---O---$H^{\delta +}$ type) and basic (E---$OH^{\delta 0}$ type) sites. For sample *III*, in the *pKa* spectrum range from 5.0 to 9.5 there is allocated a wide band corresponding to the basic (E---$OH^{\delta 0}$ type) and Bröensted acid (E---O---$H^{\delta +}$ type) sites; the band at *pKa* of 10.5 complies with the Bröensted basic sites of E---$OH^{\delta -}$ type. There are no pronounced bands on the spectrum in the *pKa* region from 0 to 12 for sample *II*; the distribution of adsorption centers is relatively even. This suggests a predominantly donor-acceptor sorption mechanism with a pevalence of electron-donor atoms on the surface of the sorbent for samples *I* and *III*. For samples *I* and *II*, an increase in *q(pKa)* value is observed in the area of Lewis acid sites (at *pKa* from 13), and in the presence of superacid sites, a coordination mechanism of sorption is possible.

Fig. 5 gives he results of TG/DTG/DSC analysis of the synthesized samples. When the samples are heated to 125–130 °C, a slight mass loss is observed and endoeffects are present on the DSC curves, most pronounced for sample *III*. The adsorption water and residual amount of probable synthesis products – ethanol, hydrochloric acid – are mainly removed in this area.

In the range of 125–375 °C there are two extremes on the DTG and DSC curves for all samples; the effects overlap each other. The total mass loss in the temperature range 125-375 °C was 34–35% for samples *I* and *III* and 45% for sample *II*.

The maxima on the DTG curves correspond to temperatures of 188 and 253 °C for samples *I* and *III;* to 211 and 238 °C for sample *II*. The maximum at 188 °C corresponds to the pure TBP decomposition (Fig. 5); this indicates that part of TBP in samples *I* and *III* is immobilized without forming a chemical bond [22–25]; the maximum at 253 °C corresponds to the oxidation of synthesis products. According to the results of *X*-ray fluorescence analysis of samples after calcination at 600–900 °C, the phosphorus content in them varies from 3.8 to 4.6% wt., which points to a partial modification of TBP during synthesis.

The main differences in the synthesis of sample *II* lied in the fact that TBP and TTC were mixed directly with an excess of the latter, which could lead to the formation of complex compounds of $SnCl_4 \cdot n$TBP type and the binding of all TBP into this compound, and the two maxima on the DTG curve — to the decomposition of these complexes.

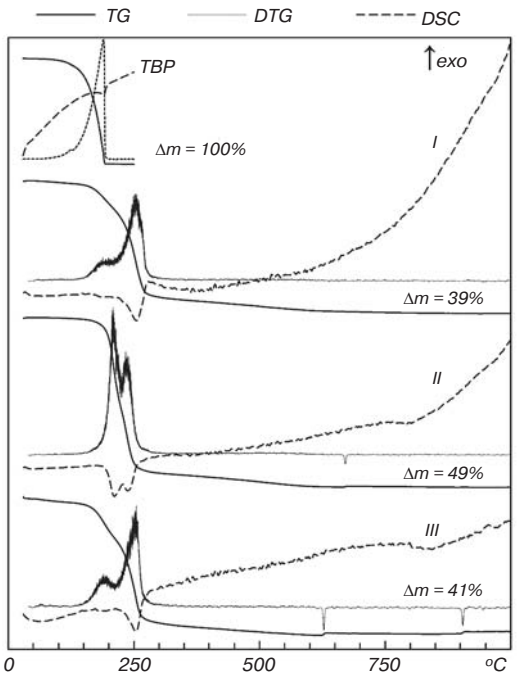

Fig. 5. TG/DTG/DSC curves of synthesized samples

At temperatures above 600 °C, several minima are present on the DTG curves for samples *II* and *III*, which correlate with a slight increase in the mass of weighted specimens (at 671 °C for sample *II*; at 628 and 904 °C for sample *III*). There are no similar sections on the DTG curve for sample *I*. Since carbon nanotubes were not used in the synthesis of sample *I*, the increase in the mass of the weighted specimens for samples *II* and *III* is apparently connected with their presence. It is known that when carbon nanotubes decompose in air at temperatures above 600 °C, their oxidation with mass loss should occur [26]; besides, the observed mass changes are not comparable with the relative mass of the introduced nanotubes. Therefore, it can be assumed that the mass increase is due to the fact that the surface of nanotubes is covered with several layers of reagents with which carbon or CO released during its combustion reacts with the participation of purge gas (air) components. These are primarily reagents used for even distribution of nanotubes (TBP for sample *II* and TEOS for sample *III*), and layers formed during slow heating of synthesis products.

Tables 3–5 present the results of testing samples in solutions of leaching of REE-containing loparite processing product.

The degree of REE extraction in the studied conditions did not exceed 72.3%, that for thorium — 58.7% (Tables 3–5). In the REE series, the maximum recovery rates are observed for samarium (52.5–72.3%) and the minimum ones for dysprosium (8.6–28.0%) and erbium (23.4–27.2%). The extraction degrees for aluminum and iron have rather high values; the highest extraction degrees were observed for iron: 88.8–92.4%.

At the same time, the value of CEC for iron (6.8–7.0 μmol/g) has lower values than for light REE (La–Nd, 8.7–84.5 μmol/g); for aluminum it is in the range of 20.4–25.3 μmol/g. Individual REE (Sm, Eu, Dy) have low values of CEC (0.1–3.2 μmol/g), which can be explained by sorption from sufficiently acidic solutions with pH = 1. It can be supposed that sorption from such solutions will achieve greater selectivity between individual REE [8].

The distribution coefficients of all elements are significantly greater than one; the largest distribution coefficients among REE were obtained for praseodymium (91.5–128.5 cm^3/g) and samarium (123.9–261.7 cm^3/g). The REE distribution coefficients for sample *II* are lower than those for samples *I* and *III*: for example, the distribution coefficient of cerium was 67.5 cm^3/g for sample *II* and 103.4 cm^3/g for sample *III*. Sample *I* is characterized by a lower thorium distribution coefficient (42.0 cm^3/g) compared to 159.4 and 115.2 cm^3/g for samples *II* and *III*, respectively.

Table 3
Indicators of element extraction using sample *I*

Indicator	Element											
	Al	Fe	Y	La	Ce	Pr	Nd	Sm	Eu	Dy	Er	Th
a, %	47.2	89.0	38.0	39.3	46.6	56.1	41.2	70.0	35.7	28.0	23.4	29.5
CEC, μmol/g	20.4	6.8	0.3	39.2	77.8	9.8	24.6	3.1	0.2	0.2	4.5	0.5
k, cm^3/g	89.9	811.4	61.7	65.1	87.7	128.5	70.5	234.5	55.8	39.1	30.6	42.0
$b_{E/La}$	1.4	12.5	0.9	1.0	1.3	2.1	1.1	3.6	0.9	0.6	0.5	0.6

Table 4
Indicators of element extraction using sample *II*

Indicator	Element											
	Al	Fe	Y	La	Ce	Pr	Nd	Sm	Eu	Dy	Er	Th
a, %	52.5	88.8	43.5	33.2	37.6	44.9	35.8	52.5	26.5	8.6	27.2	58.7
CEC, μmol/g	25.3	7.6	0.4	37.0	70.0	8.7	23.9	2.6	0.1	0.1	6.5	1.2
k, cm^3/g	123.8	892.9	86.4	55.8	67.5	91.5	62.6	123.9	40.5	10.5	41.9	159.4
$b_{E/La}$	2.2	16.0	1.5	1.0	1.2	1.6	1.1	2.2	0.7	0.2	0.8	2.9

Table 5
Indicators of element extraction using sample *III*

Indicator	Element											
	Al	Fe	Y	La	Ce	Pr	Nd	Sm	Eu	Dy	Er	Th
a, %	48.9	92.4	49.2	41.5	50.8	56.2	45.1	72.3	46.8	18.1	24.7	53.5
CEC, μmol/g	21.1	7.0	0.4	41.4	84.5	9.8	26.9	3.2	0.2	0.1	5.2	1.0
k, cm^3/g	95.8	1222.5	97.2	71.2	103.4	128.5	82.5	261.7	88.3	22.1	32.8	115.2
$b_{E/La}$	1.3	17.2	1.4	1.0	1.5	1.8	1.2	3.7	1.2	0.3	0.5	1.6

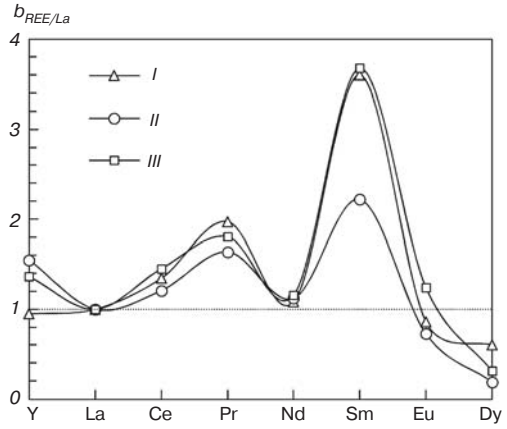

Fig. 6. REE separation coefficients relative to lanthanum depending on the atomic number

The separation coefficients of elements relative to lanthanum in ascending order of atomic number are illustrated in **Fig. 6**.

The separation coefficients obtained for sample *II* have the highest values for Fe/La pair (16.0), more than two – for part of Th/REE and REE pairs (Sm/La, Sm/Nd, Sm/Eu, REE/Dy, REE/Eu). A distinctive feature of sample *I* is the potential possibility of its application for REE isolation from thorium, but judging by the distribution coefficients of Th/REE pairs, there will also be a loss of a part of REE (Y, Pr, Sm).

The dependence of REE/La separation coefficients (Fig. 6) on the atomic number has the form of a double-humped curve. For all three samples, its general character is repeated, which points to the same basic sorption mechanism. Taking into account the data shown in Fig. 4*b*, it can be assumed that REE sorption on these samples is primarily associated with the presence of the Bröensted acid and basic sites on their surface in the region of pKa = 5.5–9.0, and the main mechanism of interaction is donor-acceptor one.

As with the extraction of TBP [27], one of the maxima on this curve corresponds to Sm/La pair, but at the same time a new maximum appears for REE pair of the light group – Pr/La. With this in mind, the separation efficiency of Pr/Nd pair increases; their separation coefficient reaches a maximum value of 1.8 for sample *I*.

Conclusions

1. Methods of sorbent synthesis based on silica and tributyl phosphate using tin chloride and nanotubes have been proposed and tested. A number of physicochemical properties have been determined for synthesized samples (*I-III*). The specific surface area and average pore size was 432 m^2/g and was 2.83 nm for sample *I* and 384 m^2/g and 3.50 nm for sample *III*. The following molecular formulas of the surface composition were calculated for the samples: $C_{90}P_{14}Si_{30}Sn_7O_{45}$ – sample *I*; $C_{132}P_4Si_4Sn_6O_{40}$ – sample *II*; $C_{85}P_{11}Si_{33}Sn_9O_{44}$ – sample *III*. According to the results of indicator analysis for samples *I* and *III*, the most intense bands in the adsorption spectra were obtained in pKa spectrum range of 4.0–9.5, which corresponds to the Bröensted acid (E---O---$H^{\delta+}$ type) and basic (E---$OH^{\delta0}$ type) sites; no pronounced bands were detected in the spectrum of sample *II*. For samples *I–II* there is observed an increase in $q(pKa)$ value at pKa from 13. This suggests a predominantly donor-acceptor sorption mechanism with a prevalence of electron-donor atoms on the sorbent surface for samples *I* and *III* as well as a possible coordination mechanism for sample *II*.

2. From the standpoint of improving the physical and mechanical characteristics, it is recommended to start the synthesis of sorbents with mixing TEOS and TBP, and then introduce TTC. The sorbents *I* and *III* synthesized under such conditions have shown great efficiency in REE extracting from process solutions of loparite working up. For example, the distribution coefficients of cerium were 87.4 and 103.4 cm^3/g for samples *I* and *III*, and 67.5 cm^3/g for sample *II*. It is also proposed to use nanotubes for reinforcements of granules (in accordance with the synthesis method for sample *III*).

3. Interesting is the possibility of preferential Sm and Pr isolation (with its separation from Nd) using sample *I*: the separation coefficients of Sm/La and Pr/La pairs were 3.6 and 2.1, respectively, and 1.8 for Pr/Nd. The separation coefficient of Sm/La pair also has a high value for sample *III* (3.7), but sample *I* is more attractive in case of REE separation from thorium ($\beta_{Th/La}$ = 0.6), although with the loss of a part of REE. In the future, it is planned to carry out some additional studies to discover the sorption mechanism.

Acknowledgments

This study was supported by the Tomsk State University Development Programme (Priority-2030).

The SEM researches and results of measuring the specific surface area (SBET) and porous structure were carried out with the equipment of Tomsk Regional Core Shared Research Facilities Center of National Research Tomsk State University. Center was supported by the Ministry of Science and Higher Education of the Russian Federation Grant no. 075-15-2021-693 (no. 13.RFC.21.0012)).

References

1. Kosynkin V. D., Moiseev S. D., Peterson C. H., Nikipelov B. V. Rare Earths Industry of Today in the Commonwealth of Independent States. *Journal of Alloys and Compounds.* 1993. Vol. 192, Iss. 1-2. pp. 118–120.

2. Gasanov A. A., Naumov A. V., Yurasova O. V., Petrov I. M., Litvinova T. E. Certain Tendencies in the Rare-Earth-Element World Market and Prospects of Russia. *Russian Journal of Non-Ferrous Metals.* 2018. Vol. 59. Iss. 5. pp. 502–511.

3. Hedrick J. B., Sinha S. P., Kosynkin V. D. Loparite, a Rare-Earth Ore (Ce, Na, Sr, Ca)(Ti, Nb, Ta, Fe^{+3})O_3. *Journal of Alloys and Compounds.* 1997. Vol. 250, Iss. 1-2. pp. 467–470.

4. Kudryavskii Y. P. Investigation of Physicochemical Fundamentals and Elaboration of the New, Improved Technology of Deactivation of Liquid Radioactive Waste of The Chlorination Process of Loparite Concentrates. *Russian Journal of Applied Chemistry*. 2011. Vol. 84, Iss. 3. pp. 515–525.

5. Tsivadze A. Y. Selective Separation of Elements of the Periodic Table with Similar Chemical Properties as a Foundation for New Technologies. *Herald of the Russian Academy of Sciences*. 2020. Vol. 90, Iss. 2. pp. 214–224.

6. Kosynkin V. D., Nikonov V. J. Rare Earth Production at the Sillamäe Plant, 1969–1991 and the Possibility of Scandium Extraction from Loparite. In Book: *Turning a Problem Into a Resource: Remediation and Waste Management at the Sillamäe Site, Estonia*. Springer, Dordrecht, 2000. P. 57–61.

7. Shulin S. S., Galieva G. N., Chighevskaya S. V., Pletuhina J. V., Saveliev N. S. Extraction Separation of Rare Earth Elements of the Medium Group with Isomolar Mixtures of Aliquat®336–TBP and Cyanex®572–TBP from Nitric Solutions. *Inorganic Materials*. 2018. Vol. 54, Iss. 5. pp. 515– 519.

8. Ehrlich G. V., Lisichkin G. V. Sorption in the Chemistry of Rare Earth Elements. Russian *Journal of General Chemistry*. 2017. Vol. 87, Iss. 6. pp. 1220–1245.

9. Xue G., Yurun F., Li M., G. Dezhi, J. Jie, Y. Jincheng, S. Haibin, G. Hongyu, Z. Yujun Phosphoryl Functionalized Mesoporous Silica for Uranium Adsorption. *Applied Surface Science*. 2017. Vol. 402. pp. 53–60.

10. Ahmed S. H. Abdel Warith A. A., Sallman A. A., El-Gammal E. M. Studies on Uranium Recovery by Activated Carbon impregnated with Tridodecylamine and Tributyl Phosphate. *Nuclear Sciences Scientific Journal*. 2018. Vol. 7, Iss. 1. pp. 189–203.

11. Mokhodoeva O. B., Myasoedova G. V., Zakharchenko E. A. Solid-phase Extractants for Radionuclide Preconcentration and Separation. New Possibilities. *Radiochemistry*. 2011. Vol. 53, Iss. 1. pp. 35–43.

12. Nekrasova N. A., Milyutin V. V., Kaptakov V. O. Solid Extractants of Russian Manufacture for the Extraction of Rare-Earth Elements and Actinides from Nitric Acid Solutions. *Transactions Kola Science Centre. Series 3: Chemistry and Materials*. 2019. Vol. 10, Iss. 1. pp. 226–229.

13. Zheng R., Bao S., Zhang Y., Chen B. Synthesis of Di-(2-ethylhexyl) Phosphoric Acid (D2EHPA)-tributyl Phosphate (TBP) Impregnated Resin and Application in Adsorption of Vanadium (IV). *Minerals*. 2018. Vol. 8, Iss. 5. pp. 206–217.

14. Naik P., Dhami P., Misra S., Jambunathan U., Mathur J. Use of Organophosphorus Extractants Impregnated on Silica Gel for the Extraction Chromatographic Separation of Minor Actinides from High Level Waste Solutions. *Journal of Radioanalytical and Nuclear Chemistry*. 2003. Vol. 257, Iss. 2. pp. 327–332.

15. Rozen A. M., Krupnov B. V. Dependence of the Extaction Ability of Orgaic Compounds on their Structure. *Russian Chemical Reviews*. 1996. Vol. 65, Iss. 11. pp. 1052–1079.

16. Grachova I. E., Karpova S. S., Moshnikov V. A., Pshchelko N. S. Netting Hierarchical Porous Structures with Electroadhesion Contacts. *Proceedings of Saint Petersburg Electrotechnical University*. 2010. No. 8. pp. 27–32.

17. Brown C. G., Sherrington L. G. Solvent Extraction Used in Industrial Separation of Rare Earths. *Journal of Chemical Technology and Biotechnology*. 1979. Vol. 29, Iss. 4. pp. 193–209.

18. Iloeje C. O. Modeling Liquid–Liquid Extraction for Critical Elements Separations: an Overview. In Book: *Multidisciplinary Advances in Efficient Separation Processes*. ACS Publications, 2020. pp. 335–365.

19. Liddell K. N. C., Bautista R. G. The Chemical Reactions of Tributyl Phosphate in the Solvent Extraction of Metals. In Book: *Hydrometallurgical Process Fundamentals*. Boston, MA: Springer, 1984. P. 429–471.

20. Mingaliov P. G., Rzhevskii D. V., Perfiliev Yu. D., Lisichkin G. V. A Mossbauer Spectroscopy Investigation of Grafted Layer of Silica Chemically Modified with Tin Compounds. *Vestnik Moskovskogo Universiteta. Seriya 2. Khimiya*. Vol. 41, No. 1. pp. 53–55.

21. Dyshin A. A., Eliseeva P. V., Bondarenko G. V., Kiselev M. G. Reinforcement of Polymethylmethacrylate of Various Molecular Weights by Diffusion Introduction of Single-walled Carbon Nanotubes in a Overcritical Carbon DIoxide Medium. *Zhurnal Fizicheskoi Khimii*. 2017. Vol. 91, No. 10. pp. 1740–1747.

22. Kamimura Y., Kurumada K. Properties and Microstructure of Silica Glass Incorporated With Tributyl Phosphate by Sol–Gel Method. *Journal of Non-Crystalline Solids*. 2009. Vol. 355, Iss. 34-36. pp. 1693–1697.

23. Higgins C. E., Baldwin W. H. The Thermal Decomposition of Tributyl Phosphate. *The Journal of Organic Chemistry*. 1961. Vol. 26, Iss. 3. pp. 846–850.

24. Horrocks A. R., Davies P. J., Kandola B. K., Alderson A. The Potential for Volatile Phosphorus-containing Flame Retardants in Textile Back-Coatings. *Journal of Fire Sciences*. 2007. Vol. 25, Iss. 6. pp. 523–540.

25. Barney G. S., Cooper T. D. The Chemistry of Tributyl Phosphate at Elevated Temperatures in The Plutonium Finishing Plant Process Vessels. Westinghouse Hanford Co., Richland, WA (United States). 1994. No. WHC-EP-0737. 65 p.

26. Pang L. S. K., Saxby J. D., Chatfield S. P. Thermogravimetric Analysis of Carbon Nanotubes and Nanoparticles. *The Journal of Physical Chemistry*. 1993. Vol. 97, Iss. 27. pp. 6941–6942.

27. McGill I., Matthey J. Rare Earth Elements. England: Technology Centre, Reading, 2000. 228 p. NFM